

Manipulating the Solvation Structure and Interface via a Bio-Based Green Additive for Highly Stable Zn Metal Anode

Yan Wang, Xiaohui Zeng,* Haiji Huang, Dongmei Xie, Jianyang Sun, Jiachang Zhao,*
Yichuan Rui, Jinguo Wang, Jodie A. Yuwono, and Jianfeng Mao*

The practical application of aqueous zinc-ion batteries (AZIBs) is limited by serious side reactions, such as the hydrogen evolution reaction and Zn dendrite growth. Here, the study proposes a novel adoption of a biodegradable electrolyte additive, γ -Valerolactone (GVL), with only 1 vol.% addition (GVL-to-H₂O volume ratio) to enable a stable Zn metal anode. The combination of experimental characterizations and theoretical calculations verifies that the green GVL additive can competitively engage the solvated structure of Zn²⁺ via replacing a H₂O molecule from [Zn(H₂O)₆]²⁺, which can efficiently reduce the reactivity of water and inhibit the subsequent side reactions. Additionally, GVL molecules are preferentially adsorbed on the surface of Zn to regulate the uniform Zn deposition and suppress the Zn dendrite growth. Consequently, the Zn anode exhibits boosted stability with ultralong cycle lifespan (over 3500 h) and high reversibility with 99.69% Coulombic efficiency. The Zn||MnO₂ full batteries with ZnSO₄-GVL electrolyte show a high capacity of 219 mAh g⁻¹ at 0.5 A g⁻¹ and improved capacity retention of 78% after 550 cycles. This work provides inspiration on bio-based electrolyte additives for aqueous battery chemistry and promotes the practical application of AZIBs.

1. Introduction

The ever-growing energy consumption and considerable decarbonization requirements call the pursuit of large-scale storage of renewable energy sources.^[1–12] Lithium-ion batteries (LIBs) have been the dominant energy storage system, however, some inherent drawbacks render them less feasible for large-scale industrial applications, such as the limited resources, high cost, and potential safety issues.^[2–5] Aqueous zinc-ion batteries (AZIBs) have emerged as a promising alternative beyond conventional LIBs due to the high specific capacity (820 mAh g⁻¹ and 5855 mAh cm⁻³), low redox potential (−0.76 V vs the standard hydrogen electrode), abundance and low toxicity of Zn metal anode.^[8–12] Nevertheless, their practical application is largely limited by the parasitic reactions such as hydrogen evolution reaction (HER) and Zn dendrite formation, which result in inferior cycling stability


and low Coulombic efficiency (CE). The H₂ generation and growth of Zn dendrites lead to continuous consumption of electrolyte and active Zn, eventually causing a short circuit, battery swelling or even battery explosion.^[13–15]

To address the aforementioned challenges of Zn metal anode, some strategies have been proposed, including separator modifications,^[16–18] anode protective coating,^[19,20] Zn-alloying metals.^[21,22] However, the preparation processes of these strategies are complicated and the manufacturing cost is relatively expensive compared to electrolyte modulation. It is well known that electrochemical behavior of Zn anode strongly relies on the electrolyte formulation and electrode-electrolyte interface. There is a direct correlation among the solvation structure of Zn-ion, water reactivity, and interface interaction. The addition of inorganic/organic molecules into conventional electrolyte is an acknowledged and facile method to optimize electrolyte composition and electrode/electrolyte interface, and thus enhancing the electrochemical performance of Zn anode.^[23–28] For example, some organic additives have a strong interaction with H₂O molecules and Zn²⁺ to break the original hydrogen bonding network and reconstruct the Zn²⁺ solvation structure, and consequently suppress the detrimental HER and by-products formation. Due to the abundant functional groups, some organic

Y. Wang, H. Huang, D. Xie, J. Sun, J. Zhao, Y. Rui, J. Wang
College of Chemistry and Chemical Engineering
Shanghai University of Engineering Science
Shanghai 201620, P. R. China
E-mail: zjc@sues.edu.cn

X. Zeng
Institute for Superconducting and Electronic Materials (ISEM)
Australian Institute for Innovative Materials (AIIM)
University of Wollongong
Wollongong, NSW 2522, Australia
E-mail: xz990@uowmail.edu.au

J. A. Yuwono, J. Mao
School of Chemical Engineering
The University of Adelaide
Adelaide, SA 5005, Australia
E-mail: jianfeng.mao@adelaide.edu.au

 The ORCID identification number(s) for the author(s) of this article can be found under <https://doi.org/10.1002/smt.202300804>

© 2023 The Authors. Small Methods published by Wiley-VCH GmbH. This is an open access article under the terms of the Creative Commons Attribution-NonCommercial License, which permits use, distribution and reproduction in any medium, provided the original work is properly cited and is not used for commercial purposes.

DOI: 10.1002/smt.202300804

molecules are prone to adsorb on electrode–electrolyte interface, which can regulate the local electric field distribution and thus enable dendrite-free Zn deposition.^[25,26] However, exploring a multifunctional electrolyte additive that simultaneously manipulates Zn²⁺ solvation structure and regulates electrode–electrolyte interface is still challenging, and the reversibility and cycling lifespans of these existing Zn electrodes remain unsatisfactory.

The ideal electrolyte additive for AZIBs is expected to not only have the capability for ensuring advanced electrochemical performance of Zn, but should also possess non-toxicity, bio-compatibility, low cost, and large-scale application prospects.^[27,28] However, most electrolyte additives employed for AZIBs were not designed with these crucial criteria in mind. Given the inherent low cost and environmental benignity of AZIBs, electrolyte additives should be consistent with the original nature of AZIBs. Therefore, the criteria for selecting electrolyte additives should not only focus on the effects of side reactions and dendrites suppression, but also the environmental friendliness and practical applications. Green and sustainable electrolyte additives are thus highly desirable for wide-scale integration of high-performance AZIBs.

Here, we report the use of biocompatible, non-toxic, and low-cost γ -Valerolactone (GVL) as a multifunctional electrolyte additive in conventional ZnSO₄ electrolyte. Only with a small amount of 1 vol.% in the electrolyte, the GVL-based electrolyte could regulate Zn²⁺ solvation structure and interface simultaneously, achieving a highly stable Zn anode. Experiments and theoretical computations verify that the GVL organic molecules have strong coordination with Zn-ions to engage the solvation structure and rearrange hydrogen bonding network, which could hinder water decomposition and by-products formation. Meanwhile, GVL additive could adsorb at the electrode-electrolyte interface to impede the deterioration of the tip effect and thus enable uniform Zn deposition. Consequently, with 1 vol.% GVL in the electrolyte, Zn||Zn symmetrical cells exhibit a prolonged cycle lifespan of over 3500 h at 1 mA cm⁻², 1 mA h cm⁻² and 650 h even at harsh condition of 10 mA cm⁻², 10 mA h cm⁻². The average coulombic efficiency remains 99.69% over 1200 cycles. The Zn||MnO₂ full batteries with 1 vol.% GVL electrolyte also exhibit superior electrochemical performance to the baseline 2 M ZnSO₄ electrolyte (BE). This simple yet effective strategy for electrolyte design opens up a green and environmentally friendly route toward the practical application of AZIBs.

2. Results and Discussion

Zn||Zn symmetric cells were utilized to evaluate the cycling stability of Zn electrodes. It should be noted that the optimal concentration of GVL is 1% by volume, as demonstrated in Figures S1–S3 (Supporting Information). **Figure 1a** shows the cycle stability of Zn electrodes in the electrolytes with and without GVL at the 1 mA cm⁻² and 1 mA h cm⁻². In the baseline electrolyte (BE) of 2 M ZnSO₄, the cells had a short circuit after only 300 hours owing to Zn dendrite. Remarkably, the symmetric cells in 1 vol.% GVL electrolyte (1% GVL) maintained stable voltage and ultra-long cycling performance for over 3500 h. The Zn electrode with 1 vol.% GVL electrolyte showed excellent long-term cycling stability and reversibility even under harsh conditions (**Figure 1b–d**). At the current density of 5 mA cm⁻² and capacity of 5 mA

h cm⁻², the symmetric cells with 1% GVL electrolyte exhibited excellent cycling stability for 1400 h (**Figure 1c**). In contrast, the cells failed after only 150 h in the BE electrolyte. Similarly, under a stricter condition (10 mA cm⁻² and 10 mA h cm⁻²), the symmetric cells still presented a longer cycle lifespan (650 h) compared to the BE electrolyte (100 h), as shown in **Figure 1d**. The excellent charge/discharge process of Zn electrode could be attributed to the inhibition effect of Zn dendrites and side reactions, which results from the introduction of GVL additive. **Figure 1e** shows the cumulative plated capacity (CPC) compared with other representative-reported works.^[29–43] Significantly, the 1% GVL electrolyte displays a high CPC of 3.25 Ah cm⁻² at 10 mA h cm⁻², which outperforms many other reported additives. These results strongly confirm the positive effect of GVL addition in boosting the electrochemical stability of the Zn electrodes. Importantly, the electrolyte with 1% GVL additive is non-flammable (**Figure S4**, Supporting Information).

The reversibility of Zn electrodes is evaluated via Zn||Cu asymmetric cells. As depicted in **Figure 2a** (**Figure S5**, Supporting Information), asymmetric Zn||Cu cells in the 1% GVL electrolyte exhibited a high average CE of 99.69% at 1 mA cm⁻² and 1 mA h cm⁻². In contrast, the CEs in the BE electrolyte displayed obvious fluctuations at around 400th cycle and decreased rapidly in the following cycles, due to generation of side reactions and Zn dendrites.^[44] As shown in **Figure 2b,c**, the CE of the 1st cycle in the BE electrolyte is 96.3%, but decreased significantly to 94.2% after 400 cycles. In contrast, the initial CE is 96.9% after the addition of GVL and remains 99.7% after 1000 cycles.

The effect of GVL additive on inhibiting side reactions and adjusting Zn deposition, was demonstrated by Linear sweep voltammetry (LSV), linear polarization test, X-ray diffraction (XRD), the scanning electron microscopy (SEM), Cyclic voltammetry (CV) and Chronoamperograms (CAs). The hydrogen evolution reaction (HER) was tested with linear sweep voltammetry (LSV) (**Figure S6**, Supporting Information). Current response occurred at -1.04 V (vs Ag/AgCl) in the BE electrolyte. In contrast, the current response occurred at -1.09 V in 1% GVL electrolyte. The negatively shifted potential evidences that the introduction of GVL into the electrolyte significantly restrained the electrochemical water decomposition. These findings were confirmed via a linear polarization test. As shown in **Figure 3a**, the Zn electrode in 1% GVL electrolytes exhibited higher corrosion voltage of -0.972 V and significantly lower corrosion current density of 2.302 mA cm⁻² than BE electrolyte (4.738 mA cm⁻²). These findings demonstrated that GVL could alleviate corrosion processes and protect the Zn anode. As illustrated in **Figure 3b**, the BE electrolyte exhibited strengthened diffraction peak of the by-product of Zn₄SO₄(OH)₆·xH₂O, derived from competitive H₂ evolution during Zn deposition and the subsequently local pH increase. The weak diffraction peak of the by-product in the 1% GVL electrolyte clarifies the inhibition effect of GVL additive on water reactivity. Moreover, the addition of GVL is favorable for Zn deposition on beneficial (002) plane, which could contribute to a dendrite-free Zn deposition.^[45,46]

To obtain the insight into the effect of GVL additive on the Zn deposition, the wettability of Zn electrode is assessed. As shown in **Figure 3c**, the contact angle of Zn foil in the BE electrolyte was measured to be high as 99.7°. In contrast, the contact angle was significantly reduced to 78.9° in 1% GVL electrolyte. These

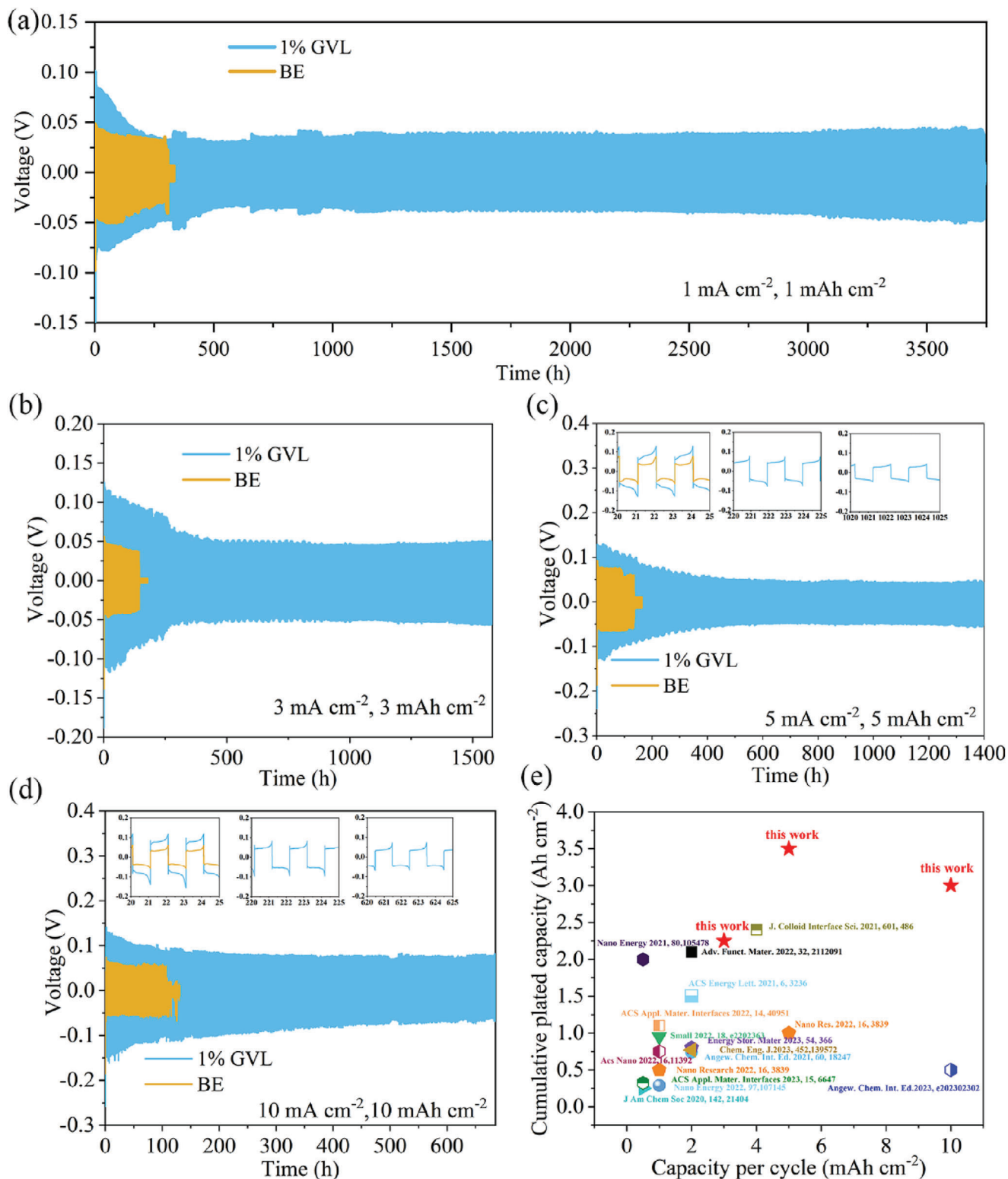


Figure 1. Cycling performance of Zn||Zn symmetric cells at a) 1 mA cm⁻², 1 mA h cm⁻², b) 3 mA cm⁻², 3 mA h cm⁻², c) 5 mA cm⁻², 5 mA h cm⁻², and d) 10 mA cm⁻², 10 mA h cm⁻². e) Cumulative plated capacity versus capacity per cycle of 1% GVL electrolyte compared with selected others.

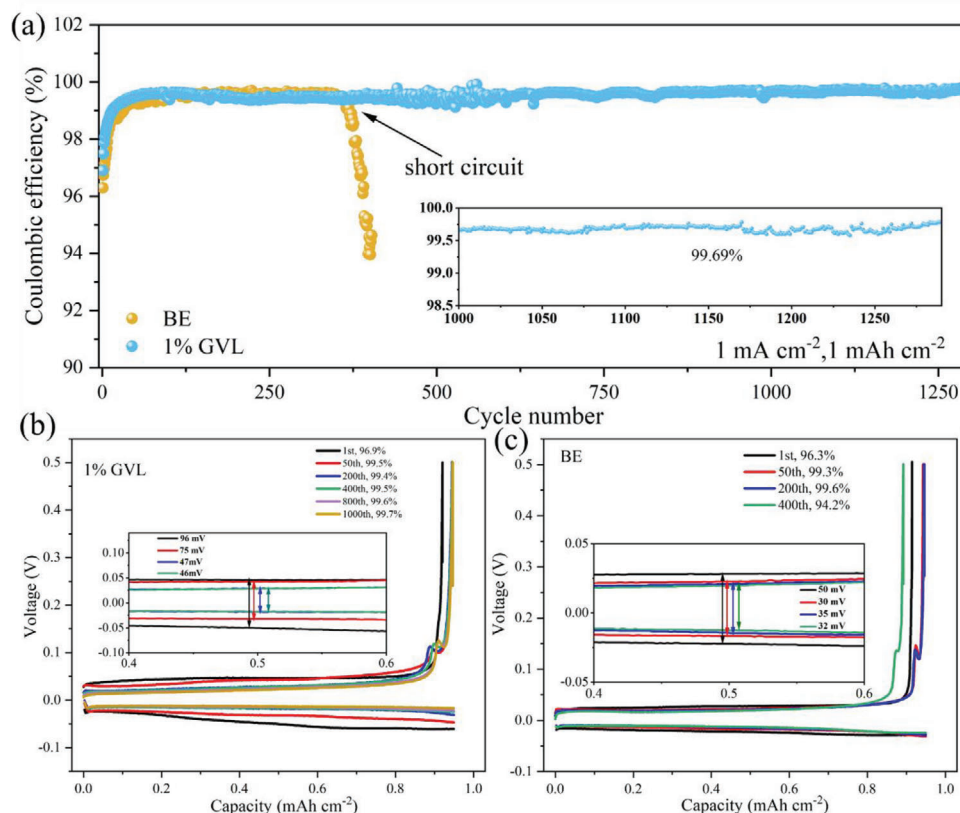


Figure 2. a) Coulomb efficiency (CE) of Zn||Cu half cells in different electrolytes. Charge/discharge voltage curves of half cells with b) 1% GVL and c) BE electrolytes, and partial enlarged view.

findings demonstrated that the GVL-containing electrolyte has favorable infiltration ability to Zn metal and thus producing homogeneous Zn plating.^[29] The plating morphology is closely related to the initial nucleation behavior. As shown in cyclic voltammetry (CV) testing results (Figure 3d), the nucleation overpotential of Zn electrode in 1% GVL electrolyte increased by 22 mV compared to that in the BE electrolyte, resulting in greater nucleation driving force and the formation of smaller Zn nuclei to inhibit random 2D diffusion and Zn dendrite formation.^[35,47,48] These results further confirmed by chronoamperometry (CA) curves. Figure 3e illustrates that in the BE electrolyte, the current response increases for 400s at a constant overpotential of -150 mV, indicating irregular dendritic Zn formation.^[49,50] In contrast, the current density increases slightly in 1% GVL electrolyte and the current response decreases. These results indicate that the GVL additive can regulate dense and uniform Zn deposition, as verified in SEM images. In BE electrolyte, the Zn surface appeared as loose and rough dendrites (Figure 3f,g). Conversely, the Zn electrode surface formed dense structure in 1% GVL electrolyte (Figure 3 h,i).

The influence of GVL molecules on the properties of ZnSO₄ electrolyte was investigated by Nuclear magnetic resonance (NMR), Raman and Fourier transform infrared spectroscopy (FTIR) spectra. As presented in Figure 4a, ²H peak shifted in the 1% GVL electrolyte compared to that in the BE electrolyte. This finding demonstrated that surrounding electronic density decreased due to the interaction between GVL and D₂O

molecules.^[32] The introduction of GVL can weaken the solvation interaction between Zn²⁺ and H₂O, which can be further confirmed by Raman and FTIR results. The decreased peak intensity and the $\nu(\text{SO}_4^{2-})$ vibration shifted in 1% GVL electrolyte indicate an impaired electrostatic coupling between Zn²⁺ and SO₄²⁻ (Figure 4b).^[35] As shown in Figure S7 (Supporting Information), the O–H vibration is between 2800 and 3800 cm⁻¹ in the Raman spectrum.^[51] The decrease in the intensity of the O–H vibrational band verified that the reactivity of H₂O molecular in 1% GVL electrolyte is much lower than that in the BE electrolyte. In addition, the FTIR spectrum also exhibited a blueshift in the O–H stretching vibration of H₂O with the increase of GVL concentration, which further proved that GVL can affect the solvation structure, as shown in Figure 4c (Figure S8, Supporting Information).^[52,53]

The radial distribution functions (RDFs) and the coordination number (N(r)) from molecular dynamics (MD) simulation were obtained to investigate solvation structure of the electrolytes. As represented in Figure 4d, in the BE electrolyte, Zn–O pair presented a sharp peak away from Zn²⁺ ≈1.94 Å in the distance. Similarly, in the GVL-containing electrolyte, the peak of Zn–O pair from the GVL molecule and water was observed also at 1.94 Å, which proved that GVL molecule can participate in the solvation structure of Zn²⁺. In addition, after the introduction of GVL additive, the N(r) of Zn²⁺ coordinated H₂O in the solvated structure decreased from 4.78 to 4.58, whereas the N(r) of GVL increased from 0 to 0.025 (Figure 4e). When the concentration

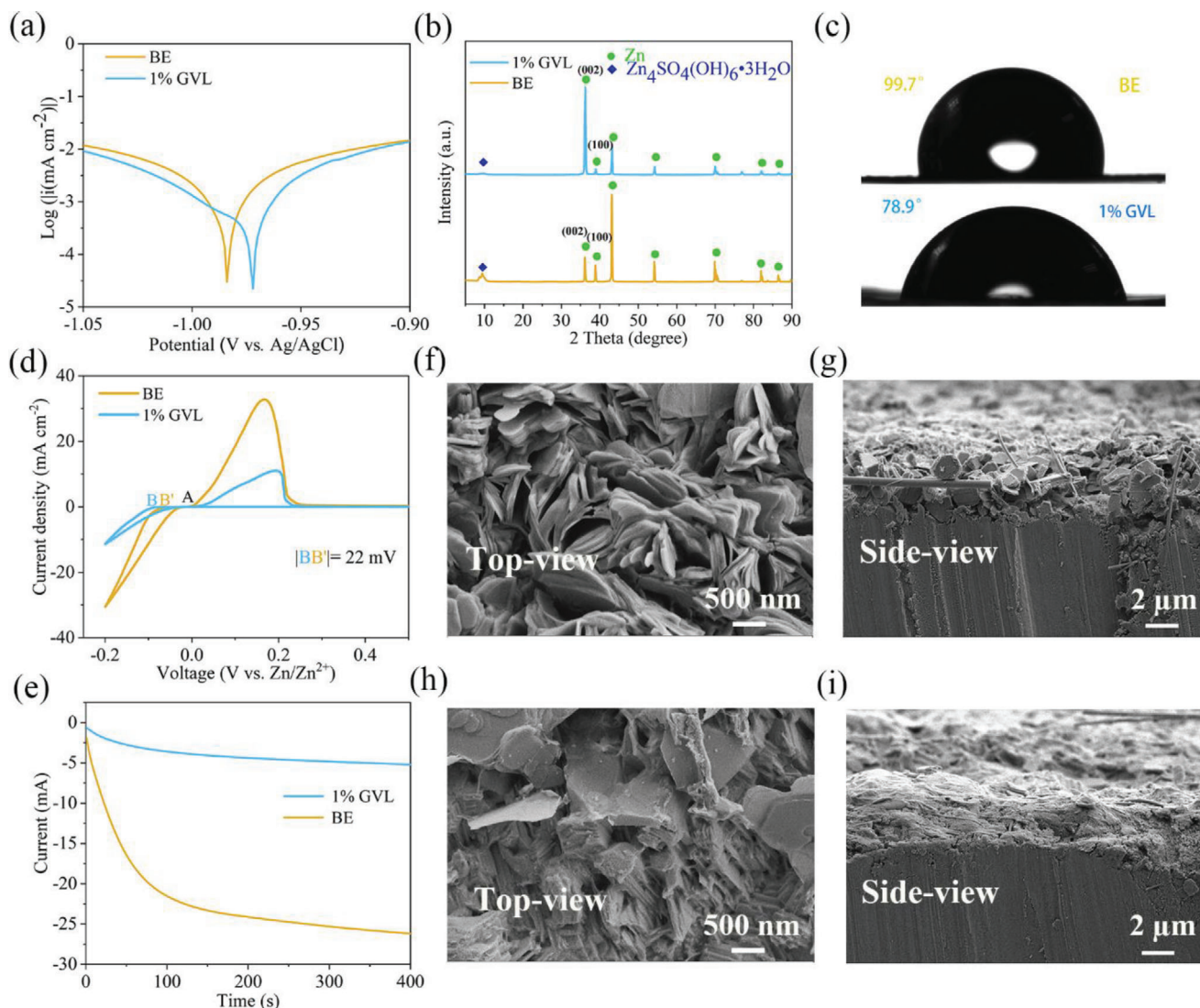


Figure 3. a) Linear polarization curves of Zn electrode. b) XRD of Zn-foil in BE and 1% GVL electrolyte for half cells after 50 cycles at 1 mA cm^{-2} , 1 mA h cm^{-2} . c) Contact angle measurement of electrolytes with Zn electrode. d) Cyclic voltammety (CV) curves of Zn||Cu half cells in the BE and 1% GVL electrolytes. e) Chronoamperograms (CAs) of Zn electrode at -150 mV . f–i) SEM images of Zn electrode after 50 cycles in f,g) BE and h,i) 1% GVL electrolyte.

of GVL increased to 20%, the value of $N(r)$ is further increased to 0.26, implying that GVL molecules are involved in the Zn^{2+} solvation structure (Figure S9, Supporting Information).^[54]

The species composition of Zn^{2+} solvation structure in the electrolytes of BE and 1% GVL was investigated (Figure 4f,g). In BE electrolyte, $[\text{Zn}(\text{H}_2\text{O})_6]^{2+}$ accounted for 40.8% of all Zn^{2+} solvated structures, whereas in 1% GVL electrolyte, $[\text{Zn}(\text{H}_2\text{O})_6]^{2+}$ accounted for 39.3% of all Zn^{2+} solvated structures. In addition, the addition of GVL increased the species composition of Zn^{2+} solvated structures. When the concentration of GVL increased further (Figure S10, Supporting Information), the content of $[\text{Zn}(\text{H}_2\text{O})_6]^{2+}$ decreased, and the presence of $[\text{Zn}(\text{H}_2\text{O})_5(\text{C}_5\text{H}_8\text{O})]^{2+}$ indicated that GVL molecules engage the solvation structure of Zn^{2+} . These results demonstrated that GVL additive breaks the original hydrogen bonding network and reconstruct the Zn^{2+} solvation structure, and

consequently suppress the decomposition of water and side reactions.

The interaction behavior of Zn^{2+} , H_2O and GVL molecules was studied by DFT calculations. The DFT calculations showed that the binding energy of Zn^{2+} -GVL is larger than that of Zn^{2+} - H_2O (Figure 4h), implying Zn^{2+} prefers to coordinate with GVL molecules rather than H_2O molecules. This result is consistent with MD simulation.^[55] The ab-initio calculations were performed to investigate and compare the adsorption energy of GVL and H_2O molecules with Zn plates. As shown in the Figure 4i, the interaction between GVL molecules and the Zn plate was stronger than that of H_2O molecules at any adsorption location, and GVL molecules were preferentially adsorbed on 002 crystal surface of Zn (GVL(P)). GVL has a greater highest occupied molecular orbital (HOMO) than that for H_2O , and thus electrons in GVL are more readily lost when absorbing on the Zn

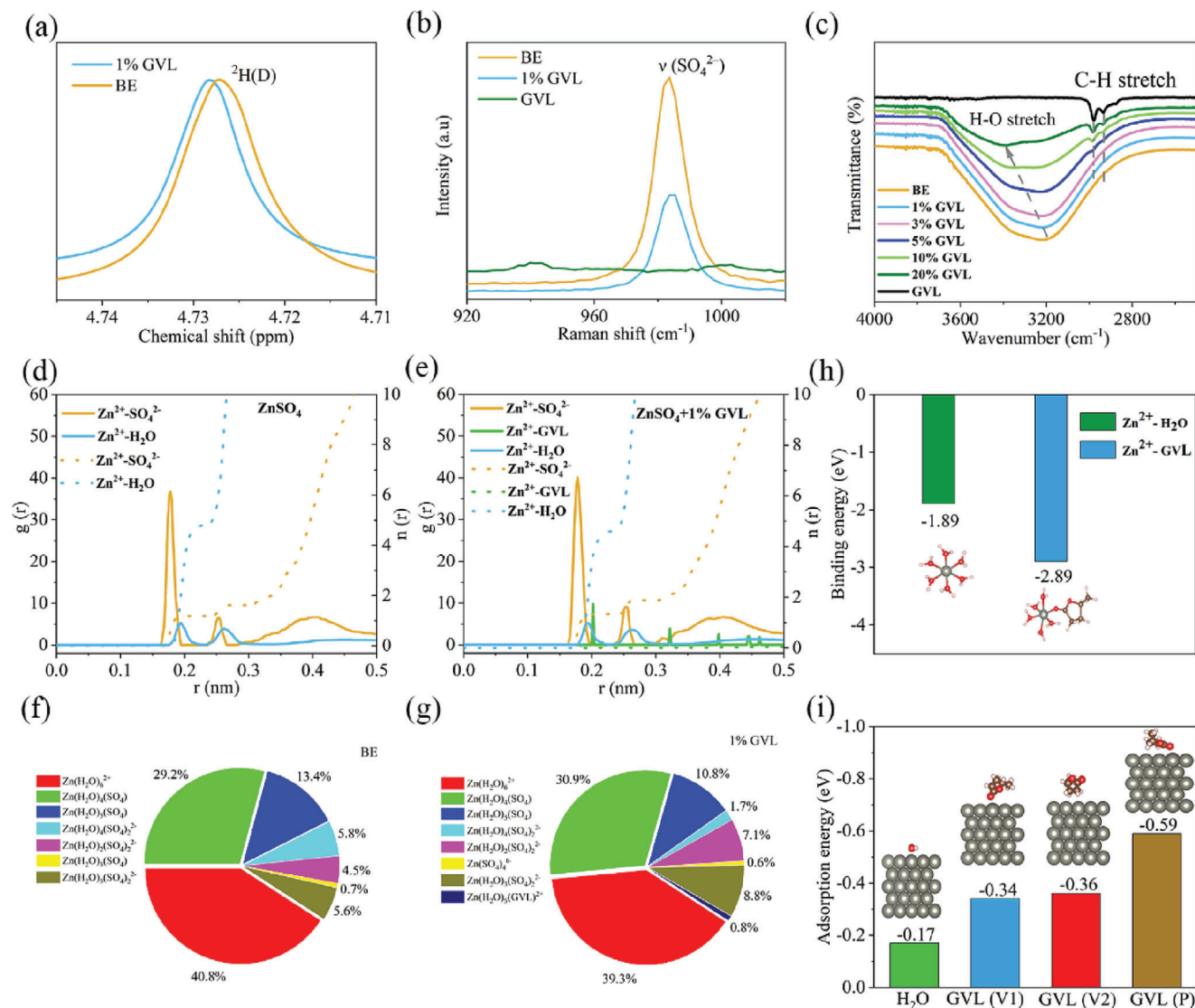


Figure 4. a) ^2H NMR spectra for BE and 1% GVL electrolyte. b) Raman spectra of BE and 1% GVL electrolyte. c) FT-IR spectra. The RDF and coordination number analyses in d) BE and e) 1% GVL. Distributions of possible Zn^{2+} solvation sheath compositions of f) BE and g) 1% GVL from MD simulation. h) Binding energy of $\text{Zn}^{2+}\text{-H}_2\text{O}$ (left) and $\text{Zn}^{2+}\text{-GVL}$ (right). i) Adsorption energy comparison of H_2O and GVL molecules on Zn (002) crystal plane.

surface and further confirming strong chemical adsorption of GVL (Figure S11, Supporting Information).^[56] The adsorption of GVL on the surface of Zn anode can produce electrostatic shielding effect, induce the uniform distribution of Zn^{2+} , and ensure dendrite-free Zn deposition.^[32] It can also be further demonstrated by electric double layer capacitance (EDLC). Compared with the BE electrolyte, the EDLC value of the electrolyte containing GVL is smaller: BE ($27.21 \mu\text{F cm}^{-2}$) > 1% GVL ($10.88 \mu\text{F cm}^{-2}$) (Figure S12, Supporting Information). The smaller EDLC indicates a greater thickness of the diffusion layer for Zn^{2+} and account for the worse reaction kinetics, further confirms the preferential adsorption of GVL on the surface of the Zn anode (Figure 4i). However, the strong interaction between GVL and Zn^{2+} ions can partially cancel the limitation for reaction kinetics from the adsorption of GVL molecules as the “smoother” for Zn deposition (Figure 4h). Thus, the GVL could be an appropriate additive

which synergically favors the smooth Zn deposition without sacrificing the reaction kinetics of Zn anodes.^[57,58]

To evaluate the practical applications of GVL additive, the Zn|| MnO_2 full cells were assembled and tested. Commercial MnO_2 powder was directly used as the cathode material (Figures S13 and S14, Supporting Information). Cyclic voltammogram (CV) curves of the full batteries with BE and 1% GVL electrolyte additive are shown in Figure 5a. The two curves exhibited similar redox pairs, demonstrating the redox reaction of MnO_2 cathode is not affected by GVL additive. Full batteries in the 1% GVL electrolyte have smaller polarization and higher current density, which indicates a faster dynamic process and higher discharge capacity.^[31,59,60] As presented in Figure 5b–d, the Zn|| MnO_2 full cell in 1% GVL electrolyte delivers superior rate performance with high capacities of 300 mA h g^{-1} at 0.1 A g^{-1} and 120 mA h g^{-1} at 2 A g^{-1} , respectively. Notably, when the

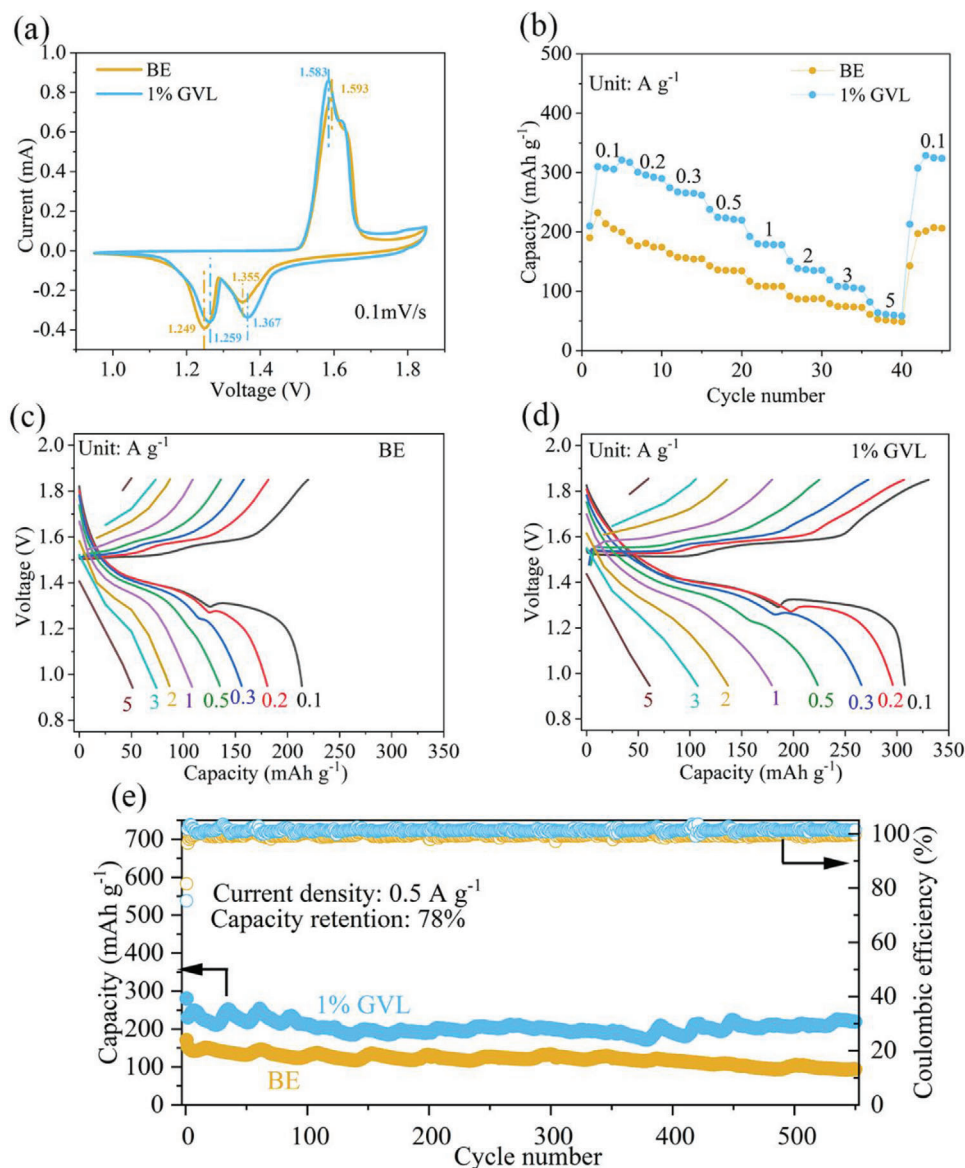


Figure 5. a) CV curves in BE and with 1% GVL. b) Rate capability at 0.1, 0.2, 0.3, 0.5, 1, 2, 3, and 5 A g^{-1} . c,d) Charge–discharge curves. e) Long-term cycling of full batteries at 0.5 A g^{-1} in BE and 1% GVL electrolyte.

rate shifted back to 0.1 A g^{-1} after high-rate cycling, the capacities recovered to $\approx 300 \text{ mA h g}^{-1}$, resulting from the suppression of side reactions and the improved stability of Zn anode in 1% GVL electrolyte. MnO_2 electrode in GVL-added electrolyte also shows better wettability (Figure S15, Supporting Information) than that in pristine ZnSO_4 electrolyte, which would facilitate the charge transport and benefit the capability of MnO_2 cathode. The long-term cycling stability of full cells were assessed at 0.5 A g^{-1} (Figure 5e). $\text{Zn}||\text{MnO}_2$ full batteries in 1% GVL electrolyte showed a greater capacity of 219 mAh g^{-1} and capacity retention of 78% after 550 cycles than that in BE electrolyte (60% retention after 550 cycles). Moreover, at high current density of 1 and 5 A g^{-1} , the $\text{Zn}-\text{MnO}_2$ full cells with 1% GVL electrolyte exhibited significantly boosted cycling performance (Figures S16 and S17, Supporting Information).

3. Conclusion

Bio-based green GVL organic molecules are introduced into ZnSO_4 electrolyte as a multifunctional additive to effectively inhibit Zn dendrites and detrimental side reactions. The additive is preferentially adsorbed at the electrode/electrolyte interface to regulate the uniform deposition of Zn. Moreover, the Combined experimental characterization and theoretical computation verify that GVL molecules have strong coordination with Zn-ions to engage the solvation structure and rearrange hydrogen bonding network, and consequently restrain the reactivity of water and by-products formation. As a result, the Zn electrode with GVL additive exhibit a prolonged cycle lifespan of over 3500 h at 1 mA cm^{-2} , 1 mA h cm^{-2} and 650 h even at 10 mA cm^{-2} , 10 mA h cm^{-2} , significantly outperforming that of the baseline electrolyte.

The average coulombic efficiency remains as high as 99.69% after 1200 cycles. In addition, Zn||MnO₂ full batteries with ZnSO₄-GVL electrolyte showed a high capacity of 219 mAh g⁻¹ at 0.5 A g⁻¹ and high capacity retention. We believe that this facile and effective additive strategy can also be extended to other aqueous battery systems and offer a novel route for the large-scale application of aqueous energy storage devices.

Supporting Information

Supporting Information is available from the Wiley Online Library or from the author.

Acknowledgements

J.Z. acknowledges the financial support from the Shanghai University of Engineering Science. J.M. acknowledges the funding support from the Australian Research Council Discovery Project (DP200101862). J.A.Y. acknowledges the high-performance computational support from the National Computing Infrastructure (NCI) Australia.

Open access publishing facilitated by The University of Adelaide, as part of the Wiley - The University of Adelaide agreement via the Council of Australian University Librarians.

Conflict of Interest

The authors declare no conflict of interest.

Data Availability Statement

The data that support the findings of this study are available from the corresponding author upon reasonable request.

Keywords

aqueous Zn-ion batteries (AZIBs), electrolyte additives, interfaces, solvation structures, zinc dendrite, Zn metal anodes

Received: June 28, 2023
Revised: August 14, 2023
Published online:

- [1] D. Larcher, J. M. Tarascon, *Nat. Chem.* **2014**, *7*, 19.
- [2] M. Li, J. Lu, Z. Chen, K. Amine, *Adv. Mater.* **2018**, *30*, 1800561.
- [3] X. Li, G. Chen, Z. Le, X. Li, P. Nie, X. Liu, P. Xu, H. B. Wu, Z. Liu, Y. Lu, *Nano Energy* **2019**, *59*, 464.
- [4] J. Wu, Y. Cao, H. Zhao, J. Mao, Z. Guo, *Carbon Energy* **2019**, *1*, 57.
- [5] M. Li, C. Wang, K. Davey, J. Li, G. Li, S. Zhang, J. Mao, Z. Guo, *Smart-Mat* **2023**, e1185, <https://doi.org/10.1002/smm2.1185>.
- [6] Q. Zhang, Z. Wang, S. Zhang, T. Zhou, J. Mao, Z. Guo, *Electrochem. Energy Rev.* **2018**, *1*, 625.
- [7] S. Liu, J. Mao, L. Zhang, W. Pang, A. Du, Z. Guo, *Adv. Mater.* **2021**, *33*, 2006313.
- [8] F. Wang, O. Borodin, T. Gao, X. Fan, W. Sun, F. Han, A. Faraone, J. A. Dura, K. Xu, C. Wang, *Nat. Mater.* **2018**, *17*, 543.
- [9] T. Zhang, Y. Tang, S. Guo, X. Cao, A. Pan, G. Fang, J. Zhou, S. Liang, *Energy Environ. Sci.* **2020**, *13*, 4625.
- [10] Y.-P. Deng, R. Liang, G. Jiang, Y. Jiang, A. Yu, Z. Chen, *ACS Energy Lett.* **2020**, *5*, 1665.
- [11] S. Liu, R. Zhang, J. Mao, J. Yuwono, C. Wang, K. Davey, Z. Guo, *Appl. Phys. Rev.* **2023**, *10*, 021304.
- [12] G. Li, L. Sun, S. Zhang, C. Zhang, H. Jin, K. Davey, G. Liang, S. Liu, J. Mao, Z. Guo, *Adv. Funct. Mater.* **2023**, 2301291, <https://doi.org/10.1002/adfm.202214538>.
- [13] L. Ma, M. A. Schroeder, O. Borodin, T. P. Pollard, M. S. Ding, C. Wang, K. Xu, *Nat. Energy* **2020**, *5*, 743.
- [14] X. Jia, C. Liu, Z. G. Neale, J. Yang, G. Cao, *Chem. Rev.* **2020**, *120*, 7795.
- [15] Y. Lyu, J. Yuwono, P. Wang, Y. Wang, F. Yang, S. Liu, S. Zhang, B. Wang, K. Davey, J. Mao, Z. Guo, *Angew. Chem., Int. Ed.* **2023**, *62*, e202303011.
- [16] J. Cao, D. Zhang, X. Zhang, M. Sawangphruk, J. Qin, R. Liu, *J. Mater. Chem. A* **2020**, *8*, 9331.
- [17] C. Li, Z. Sun, T. Yang, L. Yu, N. Wei, Z. Tian, J. Cai, J. Lv, Y. Shao, M. H. Rummeli, J. Sun, Z. Liu, *Adv. Mater.* **2020**, *32*, 2003425.
- [18] L. Yao, C. Hou, M. Liu, H. Chen, Q. Zhao, Y. Zhao, Y. Wang, L. Liu, Z. W. Yin, J. Qiu, S. Li, R. Qin, F. Pan, *Adv. Funct. Mater.* **2022**, *33*, 2209301.
- [19] Y. Cui, Q. Zhao, X. Wu, X. Chen, J. Yang, Y. Wang, R. Qin, S. Ding, Y. Song, J. Wu, K. Yang, Z. Wang, Z. Mei, Z. Song, H. Wu, Z. Jiang, G. Qian, L. Yang, F. Pan, *Angew. Chem., Int. Ed.* **2020**, *59*, 16594.
- [20] M. Gopalakrishnan, S. Ganesan, M. T. Nguyen, T. Yonezawa, S. Praserttham, R. Pornprasertsuk, S. Kheawhom, *Chem. Eng. J.* **2023**, *457*, 141334.
- [21] S. B. Wang, Q. Ran, R. Q. Yao, H. Shi, Z. Wen, M. Zhao, X. Y. Lang, Q. Jiang, *Nat. Commun.* **2020**, *11*, 1634.
- [22] Y. Zhang, J. D. Howe, S. Ben-Yoseph, Y. Wu, N. Liu, *ACS Energy Lett.* **2021**, *6*, 404.
- [23] S. Liu, J. Vongsvivut, Y. Wang, R. Zhang, F. Yang, S. Zhang, K. Davey, J. Mao, Z. Guo, *Angew. Chem., Int. Ed.* **2023**, *62*, e202215600.
- [24] Z. Liu, R. Wang, Q. Ma, J. Wan, S. Zhang, L. Zhang, H. Li, Q. Luo, J. Wu, T. Zhou, J. Mao, L. Zhang, C. Zhang, Z. Guo, *Adv. Funct. Mater.* **2023**, 2214538, <https://doi.org/10.1002/adfm.202214538>.
- [25] C. Zhang, W. Shin, L. Zhu, C. Chen, J. C. Neuefeind, Y. Xu, S. I. Allec, C. Liu, Z. Wei, A. Daniyar, J. X. Jiang, C. Fang, P. A. Greaney, X. Ji, *Carbon Energy* **2020**, *3*, 339.
- [26] Q. Zhang, Y. Ma, Y. Lu, X. Zhou, L. Lin, L. Li, Z. Yan, Q. Zhao, K. Zhang, J. Chen, *Angew. Chem., Int. Ed.* **2021**, *60*, 23357.
- [27] Y.-H. Lee, Y. Jeoun, S.-H. Lee, J. H. Kim, S.-Y. Kim, S.-H. Yu, K.-S. Ahn, Y.-E. Sung, *Chem. Eng. J.* **2023**, *464*, 142580.
- [28] F. Tao, Y. Liu, X. Ren, J. Wang, Y. Zhou, Y. Miao, F. Ren, S. Wei, J. Ma, *J. Energy Chem.* **2022**, *66*, 397.
- [29] K. Wang, T. Qiu, L. Lin, X.-X. Liu, X. Sun, *Energy Stor. Mater.* **2023**, *54*, 366.
- [30] T. Xin, R. Zhou, Q. Xu, X. Yuan, Z. Zheng, Y. Li, Q. Zhang, J. Liu, *Chem. Eng. J.* **2023**, *452*, 139572.
- [31] C. Huang, X. Zhao, Y. Hao, Y. Yang, Y. Qian, G. Chang, Y. Zhang, Q. Tang, A. Hu, X. Chen, *Adv. Funct. Mater.* **2022**, *32*, 2112091.
- [32] P. Sun, L. Ma, W. Zhou, M. Qiu, Z. Wang, D. Chao, W. Mai, *Angew. Chem., Int. Ed.* **2021**, *60*, 18247.
- [33] F. Wu, Y. Chen, Y. Chen, R. Yin, Y. Feng, D. Zheng, X. Xu, W. Shi, W. Liu, X. Cao, *Small* **2022**, *18*, e2202363.
- [34] L. Cao, D. Li, E. Hu, J. Xu, T. Deng, L. Ma, Y. Wang, X. Q. Yang, C. Wang, *J. Am. Chem. Soc.* **2020**, *142*, 21404.
- [35] R. Qin, Y. Wang, M. Zhang, Y. Wang, S. Ding, A. Song, H. Yi, L. Yang, Y. Song, Y. Cui, J. Liu, Z. Wang, S. Li, Q. Zhao, F. Pan, *Nano Energy* **2021**, *80*, 105478.
- [36] W. Zhou, M. Chen, Q. Tian, J. Chen, X. Xu, X. Han, J. Xu, *J. Colloid Interface Sci.* **2021**, *601*, 486.
- [37] Y. Cao, X. Tang, L. Li, H. Tu, Y. Hu, Y. Yu, S. Cheng, H. Lin, L. Zhang, J. Di, Y. Zhang, M. Liu, *Nano Res.* **2022**, *16*, 3839.
- [38] Z. Miao, Q. Liu, W. Wei, X. Zhao, M. Du, H. Li, F. Zhang, M. Hao, Z. Cui, Y. Sang, X. Wang, H. Liu, S. Wang, *Nano Energy* **2022**, *97*, 107145.

- [39] W. He, Y. Ren, B. S. Lamsal, J. Pokharel, K. Zhang, P. Kharel, J. J. Wu, X. Xian, Y. Cao, Y. Zhou, *ACS Appl. Mater. Interfaces* **2023**, *15*, 6647.
- [40] M. Qiu, P. Sun, G. Cui, W. Mai, *ACS Appl. Mater. Interfaces* **2022**, *14*, 40951.
- [41] M. Yan, N. Dong, X. Zhao, Y. Sun, H. Pan, *ACS Energy Lett.* **2021**, *6*, 3236.
- [42] J. Luo, L. Xu, Y. Zhou, T. Yan, Y. Shao, D. Yang, L. Zhang, Z. Xia, T. Wang, L. Zhang, T. Cheng, Y. Shao, *Angew. Chem., Int. Ed.* **2023**, *62*, e202302302.
- [43] J. Xu, W. Lv, W. Yang, Y. Jin, Q. Jin, B. Sun, Z. Zhang, T. Wang, L. Zheng, X. Shi, B. Sun, G. Wang, *ACS Nano* **2022**, *16*, 11392.
- [44] K. Zhao, F. Liu, G. Fan, J. Liu, M. Yu, Z. Yan, N. Zhang, F. Cheng, *ACS Appl. Mater. Interfaces* **2021**, *13*, 47650.
- [45] Z. Huang, Z. Li, Y. Wang, J. Cong, X. Wu, X. Song, Y. Ma, H. Xiang, Y. Huang, *ACS Energy Lett.* **2022**, *8*, 372.
- [46] H. Zhang, Y. Zhong, J. Li, Y. Liao, J. Zeng, Y. Shen, L. Yuan, Z. Li, Y. Huang, *Adv. Energy Mater.* **2022**, *13*, 2203254.
- [47] B. Wang, R. Zheng, W. Yang, X. Han, C. Hou, Q. Zhang, Y. Li, K. Li, H. Wang, *Adv. Funct. Mater.* **2022**, *32*, 2112693.
- [48] H. Lu, X. Zhang, M. Luo, K. Cao, Y. Lu, B. B. Xu, H. Pan, K. Tao, Y. Jiang, *Adv. Funct. Mater.* **2021**, *31*, 2103514.
- [49] A. Bayaguud, X. Luo, Y. Fu, C. Zhu, *Energy Environ. Sci.* **2020**, *5*, 3012.
- [50] H. Huang, D. Xie, J. Zhao, P. Rao, W. M. Choi, K. Davey, J. Mao, *Adv. Energy Mater.* **2022**, *12*, 2202419.
- [51] T. C. Li, Y. V. Lim, X. L. Li, S. Luo, C. Lin, D. Fang, S. Xia, Y. Wang, H. Y. Yang, *Adv. Energy Mater.* **2022**, *12*, 2103231.
- [52] J. Hao, L. Yuan, C. Ye, D. Chao, K. Davey, Z. Guo, S. Z. Qiao, *Angew. Chem., Int. Ed.* **2021**, *60*, 7366.
- [53] L. Geng, J. Meng, X. Wang, C. Han, K. Han, Z. Xiao, M. Huang, P. Xu, L. Zhang, L. Zhou, L. Mai, *Angew. Chem., Int. Ed.* **2022**, *61*, e202206717.
- [54] P. Xiong, Y. Kang, N. Yao, X. Chen, H. Mao, W.-S. Jang, D. M. Halat, Z.-H. Fu, M.-H. Jung, H. Y. Jeong, Y.-M. Kim, J. A. Reimer, Q. Zhang, H. S. Park, *ACS Energy Lett.* **2023**, *8*, 1613.
- [55] L. Miao, R. Wang, S. Di, Z. Qian, L. Zhang, W. Xin, M. Liu, Z. Zhu, S. Chu, Y. Du, N. Zhang, *ACS Nano* **2022**, *16*, 9667.
- [56] Y. Lin, Z. Mai, H. Liang, Y. Li, G. Yang, C. Wang, *Energy Environ. Sci.* **2023**, *16*, 687.
- [57] H. Yu, D. Chen, X. Ni, P. Qing, C. Yan, W. Wei, J. Ma, X. Ji, Y. Chen, L. Chen, *Energy Environ. Sci.* **2023**, *16*, 2684.
- [58] Y. Jin, K. S. Han, Y. Shao, M. L. Sushko, J. Xiao, H. Pan, J. Liu, *Adv. Funct. Mater.* **2020**, *30*, 2003932.
- [59] Z. Wei, X. Wang, T. Zhu, P. Hu, L. Mai, L. Zhou, *Chin. Chem. Lett.* **2023**, 108421, <https://doi.org/10.1016/j.ccllet.2023.108421>.
- [60] K. Zhu, C. Guo, W. Gong, Q. Xiao, Y. Yao, K. Davey, Q. Wang, J. Mao, P. Xue, Z. Guo, *Energy Environ. Sci.* **2023**, *16*, 3612.